

Observation of $\chi_{cJ} \rightarrow \omega\omega$ decays

M. Ablikim¹, J. Z. Bai¹, Y. Ban¹¹, J. G. Bian¹, X. Cai¹, H. F. Chen¹⁶, H. S. Chen¹, H. X. Chen¹, J. C. Chen¹, Jin Chen¹, Y. B. Chen¹, S. P. Chi², Y. P. Chu¹, X. Z. Cui¹, Y. S. Dai¹⁸, Z. Y. Deng¹, L. Y. Dong^{1a}, Q. F. Dong¹⁴, S. X. Du¹, Z. Z. Du¹, J. Fang¹, S. S. Fang², C. D. Fu¹, C. S. Gao¹, Y. N. Gao¹⁴, S. D. Gu¹, Y. T. Gu⁴, Y. N. Guo¹, Y. Q. Guo¹, Z. J. Guo¹⁵, F. A. Harris¹⁵, K. L. He¹, M. He¹², Y. K. Heng¹, H. M. Hu¹, T. Hu¹, G. S. Huang¹⁶, X. P. Huang¹, X. T. Huang¹², X. B. Ji¹, X. S. Jiang¹, J. B. Jiao¹², D. P. Jin¹, S. Jin¹, Yi Jin¹, Y. F. Lai¹, G. Li², H. B. Li¹, H. H. Li¹, J. Li¹, R. Y. Li¹, S. M. Li¹, W. D. Li¹, W. G. Li¹, X. L. Li⁸, X. Q. Li¹⁰, Y. L. Li⁴, Y. F. Liang¹³, H. B. Liao⁶, C. X. Liu¹, F. Liu⁶, Fang Liu¹⁶, H. H. Liu¹, H. M. Liu¹, J. Liu¹¹, J. B. Liu¹, J. P. Liu¹⁷, R. G. Liu¹, Z. A. Liu¹, F. Lu¹, G. R. Lu⁵, H. J. Lu¹⁶, H. M. Lu¹, J. Liu¹¹, J. B. Liu¹, J. P. Liu¹⁷, R. G. Liu¹, Z. A. Liu¹, F. Lu¹, G. R. Lu⁵, H. J. Lu¹⁶, J. G. Lu¹, C. L. Luo⁹, F. C. Ma⁸, H. L. Ma¹, L. L. Ma¹, Q. M. Ma¹, X. B. Ma⁵, Z. P. Mao¹, X. H. Mo¹, J. Nie¹, S. L. Olsen¹⁵, H. P. Peng¹⁶, N. D. Qi¹, H. Qin⁹, J. F. Qiu¹, Z. Y. Ren¹, G. Rong¹, L. Y. Shan¹, L. Shang¹, D. L. Shen¹, X. Y. Shen¹, H. Y. Sheng¹, F. Shi¹, X. Shi^{11c}, H. S. Sun¹, J. F. Sun¹, S. S. Sun¹, Y. Z. Sun¹, Z. J. Sun¹, Z. Q. Tan⁴, X. Tang¹, Y. R. Tian¹⁴, G. L. Tong¹, G. S. Varner¹⁵, D. Y. Wang¹, L. Wang¹, L. S. Wang¹, M. Wang¹, P. Wang¹, P. L. Wang¹, W. F. Wang^{1d}, Y. F. Wang¹, Z. Wang¹, Z. Y. Wang¹, Zhe Wang¹, Zheng Wang², C. L. Wei¹, D. H. Wei¹, N. Wu¹, X. M. Xia¹, X. X. Xie¹, B. Xin^{8b}, G. F. Xu¹, Y. Xu¹⁰, M. L. Yan¹⁶, F. Yang¹⁰, H. X. Yang¹, J. Yang¹⁶, Y. X. Yang³, M. H. Ye², Y. X. Ye¹⁶, Z. Y. Yi¹, G. W. Yu¹, C. Z. Yuan¹, J. M. Yuan¹, Y. Yuan¹, S. L. Zang¹, Y. Zeng⁷, Yu Zeng¹, B. X. Zhang¹, B. Y. Zhang¹, C. C. Zhang¹, D. H. Zhang¹, H. Y. Zhang¹, J. W. Zhang¹, J. Y. Zhang¹, Q. J. Zhang¹, X. M. Zhang¹, X. Y. Zhang¹², Yiyun Zhang¹³, Z. P. Zhang¹⁶, Z. Q. Zhang⁵, D. X. Zhao¹, J. W. Zhao¹, M. G. Zhao¹⁰, P. P. Zhao¹, W. R. Zhao¹, Z. G. Zhao^{1e}, H. Q. Zheng¹¹, J. P. Zheng¹, Z. P. Zheng¹, L. Zhou¹, N. F. Zhou¹, K. J. Zhu¹, Q. M. Zhu¹, Y. C. Zhu¹, Y. S. Zhu¹, Yingchun Zhu^{1f}, Z. A. Zhu¹, B. A. Zhuang¹, X. A. Zhuang¹, B. S. Zou¹

(BES Collaboration)

¹ Institute of High Energy Physics, Beijing 100049, People's Republic of China

² China Center for Advanced Science and Technology (CCAST), Beijing 100080, People's Republic of China

³ Guangxi Normal University, Guilin 541004, People's Republic of China

⁴ Guangxi University, Nanning 530004, People's Republic of China

⁵ Henan Normal University, Xinxiang 453002, People's Republic of China

⁶ Huazhong Normal University, Wuhan 430079, People's Republic of China

⁷ Hunan University, Changsha 410082, People's Republic of China

⁸ Liaoning University, Shenyang 110036, People's Republic of China

⁹ Nanjing Normal University, Nanjing 210097, People's Republic of China

¹⁰ Nankai University, Tianjin 300071, People's Republic of China

¹¹ Peking University, Beijing 100871, People's Republic of China

¹² Shandong University, Jinan 250100, People's Republic of China

¹³ Sichuan University, Chengdu 610064, People's Republic of China

¹⁴ Tsinghua University, Beijing 100084, People's Republic of China

¹⁵ University of Hawaii, Honolulu, HI 96822, USA

¹⁶ University of Science and Technology of China, Hefei 230026, People's Republic of China

¹⁷ Wuhan University, Wuhan 430072, People's Republic of China

¹⁸ Zhejiang University, Hangzhou 310028, People's Republic of China

^a Current address: Iowa State University, Ames, IA 50011-3160, USA

^b Current address: Purdue University, West Lafayette, IN 47907, USA

^c Current address: Cornell University, Ithaca, NY 14853, USA

^d Current address: Laboratoire de l'Accélérateur Linéaire, Orsay, F-91898, France

^e Current address: University of Michigan, Ann Arbor, MI 48109, USA

^f Current address: DESY, D-22607, Hamburg, Germany

Decays of $\chi_{c0,2} \rightarrow \omega\omega$ are observed for the first time using a sample of 14.0×10^6 $\psi(2S)$ events collected with the BESII detector. The branching ratios are determined to be $\mathcal{B}(\chi_{c0} \rightarrow \omega\omega) = (2.29 \pm 0.58 \pm 0.41) \times 10^{-3}$ and $\mathcal{B}(\chi_{c2} \rightarrow \omega\omega) = (1.77 \pm 0.47 \pm 0.36) \times 10^{-3}$, where the first errors are statistical and the second systematic. The significances of the two signals are 4.4σ and 4.7σ , respectively.

1. Introduction

Exclusive quarkonium decays provide an important laboratory for investigating perturbative quantum chromodynamics. Compared with J/ψ and $\psi(2S)$ decays, one has much less knowledge on $PC = ++ \chi_{cJ}$ decays. While a few exclusive decays of χ_{cJ} have been measured, many decay modes remain unknown. Current theoretical analyses of χ_{cJ} decays provide only a rough treatment of the color-octet wave function. For $\chi_{cJ} \rightarrow$ *vector vector* mode, so far only measurements of $\chi_{cJ} \rightarrow \phi\phi$ [1] and $\chi_{cJ} \rightarrow K^*(892)^0 \bar{K}^*(892)^0$ [2] are available with low statistics. Precise measurements for more channels will help in better understanding the various mechanism [3,4] of χ_{cJ} decays and the nature of $^3P_J c\bar{c}$ bound states.

Further, the decays of χ_{cJ} , especially χ_{c0} and χ_{c2} , provide a direct window on glueball dynamics in the 0^{++} and 2^{++} channels since the hadronic decays may proceed via $c\bar{c} \rightarrow gg \rightarrow q\bar{q}q\bar{q}$.

Recently, the branching ratio for $\chi_{c0} \rightarrow f_0(980)f_0(980)$ [5] has been measured by the BES collaboration. In the present analysis, a search for $\chi_{c0,2}$ decaying into $\pi^+\pi^-\pi^0\pi^+\pi^-\pi^0$ final states is carried out using 14 million $\psi(2S)$ events [6] accumulated at the upgraded BES detector (BES-II). Signals of χ_{c0} and χ_{c2} decaying to ω pairs in $\psi(2S)$ radiative decays are observed for the first time.

2. The BES detector

The Beijing Spectrometer (BES) is a conventional solenoidal magnet detector that is described in detail in Ref. [7]; BESII is the upgraded version of the BES detector [8]. A 12-layer vertex chamber (VC) surrounding the beam pipe provides trigger and position information. A forty-layer main drift chamber (MDC), located radially outside the VC, provides trajectory and energy loss (dE/dx) information for charged tracks over 85% of the total solid angle. The momentum resolution is $\sigma_p/p = 0.017\sqrt{1+p^2}$ (p in GeV/c), and the dE/dx resolution for hadron tracks is $\sim 8\%$. An array of 48 scintillation counters surrounding the MDC measures the time-of-

flight (TOF) of charged tracks with a resolution of ~ 200 ps for hadrons. Outside of the TOF counters is a 12-radiation-length barrel shower counter (BSC) comprised of gas proportional tubes interleaved with lead sheets. This measures the energies of electrons and photons over $\sim 80\%$ of the total solid angle with an energy resolution of $\sigma_E/E = 22\%/\sqrt{E}$ (E in GeV). Outside of the solenoidal coil, which provides a 0.4 Tesla magnetic field over the tracking volume, is an iron flux return that is instrumented with three double layers of counters that identify muons of momentum greater than 0.5 GeV/c.

A GEANT3 based Monte Carlo (MC) program with detailed consideration of the detector performance (such as dead electronic channels) is used to simulate the BESII detector. The consistency between data and Monte Carlo has been carefully checked in many high purity physics channels, and the agreement is quite reasonable [9].

3. Event selection

3.1. $\omega\omega$ signal

In this analysis, $\chi_{cJ} \rightarrow \omega\omega \rightarrow \pi^+\pi^-\pi^0\pi^+\pi^-\pi^0$ channels are investigated using $\psi(2S)$ radiative decays to χ_{cJ} . Events with four charged tracks and five or six photons are selected. Each charged track is required to be well fit by a three-dimensional helix and to have a polar angle, θ , within the fiducial region $|\cos\theta| < 0.8$. To ensure tracks originate from the interaction region, we require $V_{xy} = \sqrt{V_x^2 + V_y^2} < 2$ cm and $|V_z| < 20$ cm, where V_x , V_y , and V_z are the x , y and z coordinates of the point of closest approach of each track to the beam axis.

A neutral cluster is considered to be a photon candidate if it is located within the BSC fiducial region ($|\cos\theta| < 0.8$), the energy deposited in the BSC is greater than 40 MeV, the first hit appears in the first 10 radiation lengths, and the angle between the cluster and the nearest charged track is greater than 6° .

A six constraint (6-C) kinematic fit to the hypothesis $\psi(2S) \rightarrow \gamma\pi^+\pi^-\pi^0\pi^+\pi^-\pi^0$ with the invariant mass of the two photon pairs constrained to the π^0 mass is performed, and the χ^2 of the 6-C fit is required to be less than 15. For events with

six photons candidates, the combination having the minimum χ^2 is chosen, and the probability of the 6-C fit is required to be larger than that of the 7-C fit to the hypothesis $\psi(2S) \rightarrow 2\pi^+2\pi^-3\pi^0$ to suppress potential background from $\psi(2S) \rightarrow \omega\pi^+\pi^-\pi^0\pi^0 \rightarrow 2\pi^+2\pi^-3\pi^0$.

Since there are four ω pair combinations from $\pi^+\pi^-\pi^0\pi^+\pi^-\pi^0$, the ω pair with the minimum R , which is defined as

$$R = \sqrt{(M_{\pi^+\pi^-\pi^0}^1 - 0.783)^2 + (M_{\pi^+\pi^-\pi^0}^2 - 0.783)^2},$$

is chosen for further analysis. Here, $M_{\pi^+\pi^-\pi^0}$ is the invariant mass of three pions and superscript 1, 2 denote different pion combinations. Therefore, there is only one entry for each event.

Figures 1 and 2 show mass distributions for candidate events in the high mass ($M_{6\pi} > 3.2$ GeV/c^2) and low mass regions ($M_{6\pi} < 3.2$ GeV/c^2), respectively. Here (a) is the scatter plot of $M_{\pi^+\pi^-\pi^0}$ versus $M_{\pi^+\pi^-\pi^0}$, (b) is the $M_{\pi^+\pi^-\pi^0}$ distribution recoiling against the opposite ω , selected by requiring $|M_{\pi^+\pi^-\pi^0} - 783| < 50$ MeV/c^2 , and (c) is the $M_{\omega\omega}$ invariant mass distribution for events in the ω pair signal region, defined by $R < 50$ MeV/c^2 . In Fig. 1, clear ω signal can be seen in (b), and clear χ_{c0} and χ_{c2} signals in (c), indicating the existence of $\chi_{c0,2} \rightarrow \omega\omega$ decays. By contrast, in the low $M_{6\pi}$ mass region, shown in Fig. 2, the ω pair signal is less significant than in the high mass region. Here, only ω pair events in high mass region are studied.

In order to test if the selection criteria in this analysis will give ‘fake’ ω pair events from non- ω pair events, 300000 MC simulated $\psi \rightarrow \gamma\chi_{c0} \rightarrow \gamma 6\pi$ events are generated in which $\chi_{c0} \rightarrow 6\pi$ decays according to the phase space. Fig. 3 shows the $M_{\pi^+\pi^-\pi^0}$ distributions of the surviving MC phase space events after requiring the same selection criteria as for the real data. No peak around the ω mass is seen, which shows that the ω pair selection criteria in this analysis does not generate fake ω pair signals.

The annular region around the ω pair signal circle, shown in Fig 1(a), is taken as the sideband region. Fig. 4 shows the $M_{6\pi}$ sideband distributions defined using the radius R to be (a) $150 < R < 300$ MeV/c^2 and (b) $100 < R < 200$

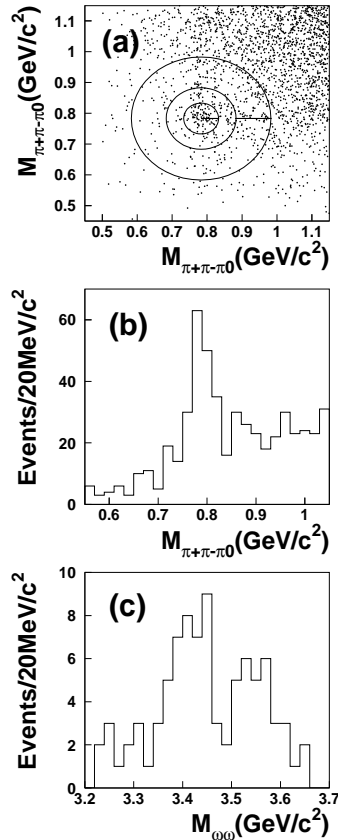


Figure 1. Distributions of events surviving the selection criteria described in the text with $M_{6\pi} > 3.2$ GeV/c^2 . (a) $M_{\pi^+\pi^-\pi^0}$ versus $M_{\pi^+\pi^-\pi^0}$, (b) $M_{\pi^+\pi^-\pi^0}$ recoiling against the opposite ω , selected by requiring $|M_{\pi^+\pi^-\pi^0} - 783| < 50$ MeV/c^2 , and (c) $M_{\omega\omega}$ invariant mass distribution for events where the ω pair satisfies $R < 50$ MeV/c^2 .

MeV/c^2 . No obvious χ_{cJ} signals seen in these sideband distributions.

3.2. MC simulation

A MC simulation of $\psi(2S) \rightarrow \gamma\chi_{cJ}$, $\chi_{cJ} \rightarrow \omega\omega$ is used to determine the detection efficiency. The proper angular distributions of the photon emit-

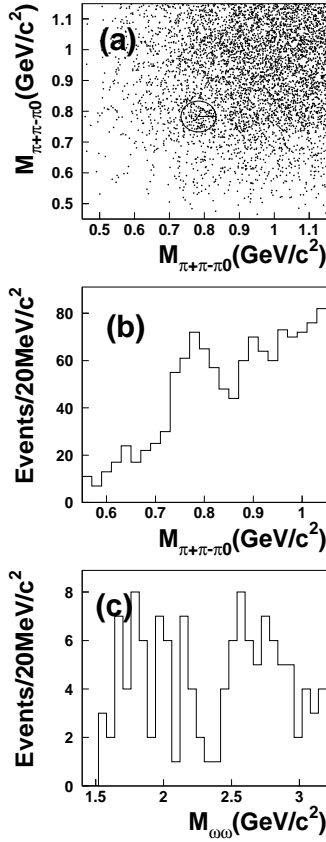


Figure 2. Distributions defined as in Fig. 1 but with $M_{6\pi} < 3.2 \text{ GeV}/c^2$.

ted in $\psi(2S) \rightarrow \gamma\chi_{cJ}$ are used [10]. Fig. 5 shows the distributions, identical to those in Fig. 1 for MC simulated $\psi(2S) \rightarrow \gamma\chi_{c0}$, $\chi_{c0} \rightarrow \omega\omega$ events passing the same selection criteria as for the real data. MC simulated $\psi(2S) \rightarrow \gamma\chi_{c2}$, $\chi_{c2} \rightarrow \omega\omega$ events have similar distributions.

3.3. Mass spectrum fit

The Maximum Likelihood (ML) method is used to fit the $M_{\omega\omega}$ mass spectrum of events in the ω pair signal region (Fig. 1(c)). The $\chi_{0,2}$ signal functions are determined from MC simulation, as shown in Fig. 5(c) for χ_{c0} , while the background

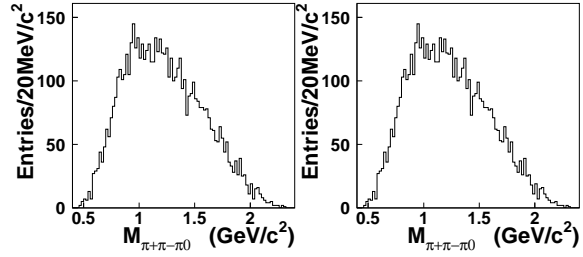


Figure 3. $M_{\pi^+\pi^-\pi^0}$ distributions from MC phase space simulated $\psi(2S) \rightarrow \gamma\chi_{c0}$, $\chi_{c0} \rightarrow \pi^+\pi^-\pi^0\pi^+\pi^-\pi^0$.

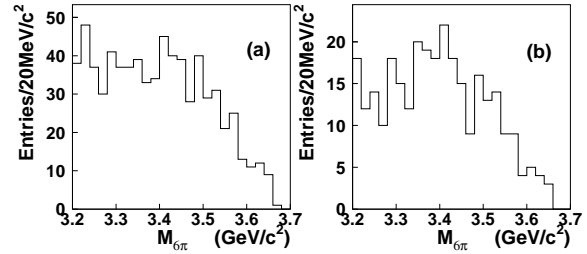


Figure 4. $M_{6\pi}$ distribution of events in sideband regions (a) $150 < R < 300 \text{ MeV}/c^2$ and (b) $100 < R < 200 \text{ MeV}/c^2$.

function is taken from the sideband distribution, shown in Fig 4(a). The fit result is represented by the solid curve in Fig. 6, and the fit yields

$$N_{\chi_{c0}} = 38.1 \pm 9.6, \quad N_{\chi_{c2}} = 27.7 \pm 7.4.$$

The statistical significances of χ_{c0} and χ_{c2} are 4.4σ and 4.7σ , respectively, which are estimated from $\sqrt{2\Delta\ln\mathcal{L}}$, where $\Delta\ln\mathcal{L}$ is the difference between the logarithmic ML values of the fit with and without the corresponding signal function.

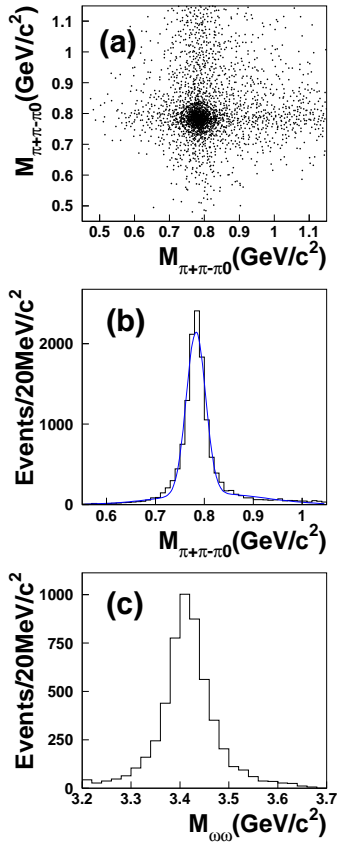


Figure 5. Distributions defined as in Fig. 1 from MC simulated $\psi(2S) \rightarrow \gamma\chi_{c0}$, $\chi_{c0} \rightarrow \omega\omega$ events.

4. Systematic error

The systematic error in this branching ratio measurement includes the uncertainties in the MDC tracking efficiency, photon efficiency, kinematic fit, background shape, number of $\psi(2S)$ events, etc.

4.1. MDC tracking efficiency and photon efficiency

For charged tracks, the uncertainty of the tracking efficiency is determined by comparing data and MC for some very clean J/ψ decay channels [9], and an error of 2% is found for each track.

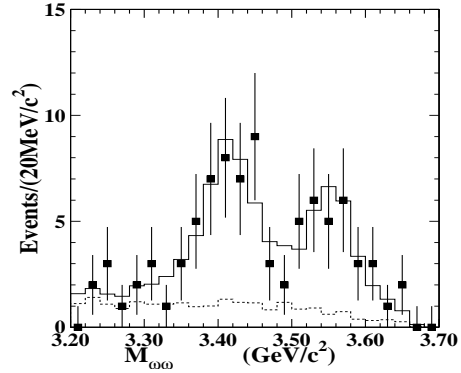


Figure 6. Fit of the $M_{\omega\omega}$ distribution. Dots with error bars are data, the solid histogram represents the maximum likelihood fit result, and the dashed histogram is the sideband background.

A similar comparison has also been performed for photons [12], and the difference is also about 2% for a single photon.

4.2. Kinematic fit

The systematic error associated with the kinematic fit is due to differences between data and MC simulation in the determination of the track momentum, the track fitting error matrix, and the photon energy and direction. The effect is studied for charged tracks and neutral tracks separately. By comparing the number of events before and after the kinematic fit for very clean event samples for data and MC simulated data, the difference is determined to be 8.4%, which is taken as the systematic error.

4.3. Background shape

Two different sideband $M_{6\pi}$ spectrum shapes, shown in Fig. 4, are used as the background function. The difference in the number of $\chi_{c0,2}$ events obtained with the two different shapes is taken as a systematic error.

4.4. Binning, fit range, and signal region

The differences caused by different binning and fit ranges in the $\omega\omega$ mass spectrum fit are 1.2% and 3.4% for χ_{c0} and χ_{c2} , respectively. Differ-

Table 1
Individual sources and total systematic error (%).

Source	$\chi_{c0} \rightarrow \omega\omega$	$\chi_{c2} \rightarrow \omega\omega$
track efficiency	8	8
photon efficiency	10	10
6-C fit	8.4	8.4
background shape	6.0	1.0
signal region	3.4	4.3
binning and fit range	1.4	3.2
angular distribution	–	9.4
No. of $\psi(2S)$ events	4	4
$\mathcal{B}(\psi(2S) \rightarrow \gamma\chi_{cJ})$	5.1	6.7
$\mathcal{B}(\omega \rightarrow 3\pi)$	0.9	0.9
$\mathcal{B}(\pi^0 \rightarrow \gamma\gamma)$	0.0	0.0
Total	18.1	20.4

ent sized signal regions yield differences of 3.1% and 2.4% for χ_{c0} and χ_{c2} , respectively, which are taken as a systematic error.

4.5. Angular distribution of $\chi_{cJ} \rightarrow \omega\omega$

In the estimation of the efficiency, a phase space generator with only the angular distribution of the radiative photon is considered. While this is correct for χ_{c0} decays, it may introduce bias for χ_{c2} decays. The effect is estimated by generating different angular distributions of the omega in the χ_{c2} rest frame. The efficiency difference between these tests and the phase space generator is estimated to be 9.4%, which is put into the systematic error.

4.6. Branching ratios of intermediate states

The errors on intermediate state branching ratios are obtained from the PDG [13] except for $\mathcal{B}(\psi(2S) \rightarrow \gamma\chi_{cJ})$, where recent CLEO results [14] are used. Table 1 summarizes all contributions to the systematic errors, and the total systematic error is determined by the quadratic sum of all terms.

5. Results

The branching ratio of $\mathcal{B}(\chi_{cJ} \rightarrow \omega\omega)$ is determined from

$$\mathcal{B}(\chi_{cJ} \rightarrow \omega\omega) = \frac{N_{\chi_{cJ}}^{obs}}{N_{\psi(2S)} \cdot f_1 \cdot f_2^2 \cdot f_3^2 \cdot \epsilon}$$

where $N_{\chi_{cJ}}^{obs}$ is the number of events selected, $N_{\psi(2S)}$ the total number of $\psi(2S)$ events, ϵ is the detection efficiency for the investigated channel, and f_1, f_2 and f_3 are the branching ratios of $\psi(2S) \rightarrow \gamma\chi_{cJ}, \omega \rightarrow 3\pi$, and $\pi^0 \rightarrow \gamma\gamma$, respectively. Table 2 lists the $\chi_{c0,2} \rightarrow \omega\omega$ branching ratio results, together with numbers used in the branching ratio calculation.

In summary, $\omega\omega$ signals in the decay of $\chi_{c0,2}$ are observed, and their branching ratios measured for the first time. χ_{c0} and χ_{c2} decays to $\omega\omega$ have similar decay branching ratios, which is different from other $\chi_{cJ} \rightarrow VV$ decays ($\chi_{cJ} \rightarrow \phi\phi, \bar{K}^*(892)^0 K^*(892)^0$). This measurement, together with previous measurements of $\chi_{cJ} \rightarrow VV$, will be helpful in understanding the nature of χ_{cJ} states.

6. Acknowledgements

The BES collaboration thanks the staff of BEPC for their hard efforts. This work is supported in part by the National Natural Science Foundation of China under contracts Nos. 10491300, 10225524, 10225525, 10425523, the Chinese Academy of Sciences under contract No. KJ 95T-03, the 100 Talents Program of CAS under Contract Nos. U-11, U-24, U-25, and the Knowledge Innovation Project of CAS under Contract Nos. U-602, U-34 (IHEP), the National Natural Science Foundation of China under Contract No. 10225522 (Tsinghua University), and the Department of Energy under Contract No.DE-FG02-04ER41291 (U Hawaii).

REFERENCES

1. BES Collaboration, J. Z. Bai *et al.*, Phys. Rev. D60, (1999) 072001.
2. BES Collaboration, M. Ablikim *et al.*, Phys. Rev. D70, (2004) 092003.

Table 2
Branching ratio results and relevant numbers.

Quantity	$\chi_{c0} \rightarrow \omega\omega$	$\chi_{c2} \rightarrow \omega\omega$
number of events	38.1 ± 9.6	27.7 ± 7.4
efficiency (%)	1.66	1.55
$N_{\psi(2S)} (\times 10^6)$	14.00 ± 0.56	14.00 ± 0.56
$\mathcal{B}(\omega \rightarrow \pi^+ \pi^- \pi^0)$ (%)	89.1 ± 0.7	89.1 ± 0.7
$\mathcal{B}(\pi^0 \rightarrow \gamma\gamma)$ (%)	98.798 ± 0.032	98.798 ± 0.032
$\mathcal{B}(\psi(2S) \rightarrow \chi_{cJ})$ (%)	9.22 ± 0.47	9.33 ± 0.63
$\mathcal{B}(\chi_{cJ} \rightarrow \omega\omega) \cdot \mathcal{B}(\psi(2S) \rightarrow \chi_{cJ}) (\times 10^{-4})$	$2.12 \pm 0.53 \pm 0.37$	$1.65 \pm 0.44 \pm 0.32$
$\mathcal{B}(\chi_{cJ} \rightarrow \omega\omega) (\times 10^{-3})$	$2.29 \pm 0.58 \pm 0.41$	$1.77 \pm 0.47 \pm 0.36$

3. C. Amsler and F. Close, Phys. Rev. D53 (1996) 295.
4. H. Q. Zhou, R. G. Ping, B. S. Zou, Phys.Lett. B611 (2005) 123
5. BES Collaboration, M. Ablikim *et al.*, Phys. Rev. D70 (2004) 092002.
6. X. H. Mo *et al.*, HEP&NP, 28 (2004) 455 (in Chinese).
7. J. Z. Bai *et al.*, BES Collab., Nucl. Instr. Meth. A344 (1994) 319.
8. J. Z. Bai *et al.*, BES Collab., Nucl. Instr. Meth. A458 (2001) 427.
9. BES Collaboration, M. Ablikim *et al.*, accepted by Nucl. Instr. Meth. A.
10. Mark-I Collaboration, W. Tanenbaum *et al.*, Phys. Rev. D17 (1978) 1731; G. Karl, S. Meshkov, and J. L. Rosner, *ibid* 13 (1976) 1203; Crystall Ball Collaboration, M. Oreglia *et al.*, *ibid* 25 (1982) 2259.
11. BES Collaboration, J. Z. Bai, *et al.*, Phys. Rev. D70 (2004) 042005.
12. S. M. Li, *et al.*, HEP&NP, 28 (8), (2004) 859 (in Chinese)
13. Particle Physics Group, S. Eidelman *et al.*, Phys. Lett. B592 (2004) 814-835.
14. CLEO Collaboration, S. B. Athar, *et al.*, Phys. Rev. D70 (2004) 112002.